J. Geogr. Sci. 2019, 29(3): 432-448
DOI: https://doi.org/10.1007/s11442-019-1608-z

Simulating runoff generation and its spatial correlation with environmental factors in Sancha River Basin:
The southern source of the Wujiang River

HOU Wenjuan, *GAO Jiangbo

Key Laboratory of Land Surface Pattern and Simulation, Institute of Geographic Sciences and Natural Resources Research, CAS, Beijing 100101, China

Abstract: Runoff generation is an important part of water retention service, and also plays an important role on soil and water retention. Under the background of the ecosystem degradation, which was caused by the vulnerable karst ecosystem combined with human activity, it is necessary to understand the spatial pattern and impact factors of runoff generation in the karst region. The typical karst peak-cluster depression basin was selected as the study area. And the calibrated and verified Soil and Water Assessment Tool (SWAT) was the main techniques to simulate the runoff generation in the typical karst basin. Further, the spatial variability of total/surface/groundwater runoff was analyzed along with the methods of gradient analysis and local regression. Results indicated that the law of spatial difference was obvious, and the total runoff coefficients were 70.0%. The groundwater runoff was rich, about 2–3 times the surface runoff. Terrain is a significant factor contributing to macroscopic control effect on the runoff service, where the total and groundwater runoff increased significantly with the rising elevation and slope. The distribution characteristics of vegetation have great effects on surface runoff. There were spatial differences between the forest land in the upstream and orchard land in the downstream, in turn the surface runoff presented a turning point due to the influence of vegetation. Moreover, the results of spatial overlay analysis showed that the highest value of total and groundwater runoff was distributed in the forest land. It is not only owing to the stronger soil water retention capacity of forest ecosystem, and geologic feature of rapid infiltration in this region, but also reflected the combining effects on the land cover types and topographical features. Overall, this study will promote the development and innovation of ecosystem services fields in the karst region, and further provide a theoretical foundation for ecosystem restoration and reconstruction.

Keywords: runoff generation; SWAT; spatial variation; impact factors; karst ecosystem

Received: 2018-07-12 **Accepted:** 2018-08-17

Foundation: National Basic Research Program of China, No.2015CB452702; National Natural Science Foundation of China, No.41671098, No.41530749; "Strategic Priority Research Program" of the Chinese Academy of Sciences, No.XDA20020202; Open Foundation of Laboratory for Earth Surface Processes (LESP) Ministry of Education

Author: Hou Wenjuan, PhD, specialized in research on karst ecosystem services. E-mail: houwj.13b@igsnrr.ac.cn

***Corresponding author:** Gao Jiangbo, PhD, E-mail: gaojiangbo@igsnrr.ac.cn

1 Introduction

Ecosystem services refer to the environmental conditions and utility provided and maintained by ecosystems, on which humans rely for survival and development (Daily, 1997). Bridging the natural and social systems, ecosystem services are a key research topic in ecology and geography, and receive significant attention from researchers and scientific organizations (Fu *et al*., 2013; Fu and Zhang, 2014; Li, 2014). According to their utility, ecosystem services can be classified into supporting, provisioning, regulating, and cultural services (Costanza *et al*., 1997; Fu and Yu, 2016). The Millennium Ecosystem Assessment Report, however, highlighted that 60% of key ecosystem service items around the world have deteriorated since the late 20th century (among 24 global ecosystem services evaluated, 15 of them are deteriorating) and problems related to regulating services have become more severe (MEA, 2005). Water retention is an important ecosystem service that covers water supply and regulation. It plays an essential role in many aspects, such as maintaining ecological safety and ensuring a high quality of life for humans. Due to water cycle processes and water mass balances, different water retention indicators are closely related and interact with each other (Liu and Du, 1985). For example, water generation (i.e. water resource provisioning services) significantly affects other services such as soil moisture regulation and flood regulation and storage.

In southwest China, special geologic conditions and interconnected surface and subsurface hydrological systems result in fragile karst ecosystems. Global climate change and anthropogenic interference have led to serious vegetation deterioration and accelerated soil erosion, which eventually resulted in rocky desertification (Pan and Lu, 2010; Li *et al*., 2016). This severely hinders sustainable development and ecological civilization construction in southwest China (Yuan, 2015). Soil and water loss is the core issue behind rocky desertification (Bai and Wang, 2011), soil and water conservation (soil moisture retention and soil conservation) in karst areas is critical to prevent rocky desertification and to promote ecological restoration. Runoff processes provide water resources for humans and are essential for soil moisture and soil conservation. Studies on runoff generation services in typical karst areas are beneficial for strengthening the water-retention and soil-fixing capacity in karst areas, and enable analysis of the weighted relationship between runoff generation and soil moisture retention, providing theoretical evidence for rocky desertification control and ecological restoration.

At present, studies on the karst runoff generation focus either on the macroscopic scale, where the total volume and value of water retention are calculated using empirical formulae or value equivalent methods based on water balance theories (Zhang *et al*., 2011), or at the plot scale, where dynamic pattern analysis of eco-hydrological processes (Chen *et al*., 2013; Dai *et al*., 2017) reveals the factors contributing to runoff processes (Hu *et al*., 2012). However, highly heterogeneous landscapes in karst areas lead to remarkable spatial differences in runoff generation. It is difficult to upscale the empirical patterns observed at observation plots to the regional scale. Empirical formulae and value equivalent methods also do not consider the physical mechanisms and spatial patterns of runoff volumes (Zhang *et al*., 2013), which should be the main focus in karst areas with relatively high landscape fragmentation. Conversely, the Soil and Water Assessment Tool (SWAT) model is based on

physical mechanisms and depicts some processes using empirical models. Thus, it is widely employed in runoff studies under different environments (Zhou *et al*., 2013; Lv *et al*., 2014; Xu *et al*., 2015). In particular, its simplified calculation method makes the SWAT model somewhat applicable to karst areas, where the underlying surface conditions are complicated, and hydrogeological conditions are unusual (Wang *et al*., 2014; Tian *et al*., 2016). Therefore, this study uses the SWAT model to simulate runoff generation services in a typical karst drainage basin. Spatial variation characteristics are examined by various topographic background and land cover systems in order to promote the development of karst ecosystem services research, and to provide theoretical support for regional sustainable development.

2 Study area

The Sancha River is a primary tributary of the southern source of the Wujiang River, lying between 104°54′–106°24′E and 26°06′–27°00′N with a drainage area of 4681 km^2. It originates from Wumeng Mountain in west Guizhou. In Dongfeng Reservoir in Qianxi county, Bijie city, the Sancha River joins the Liuchong River, a primary tributary of the northern source of the Wujiang River, to form the Yachi River in the midstream of the Wujiang River. The Sancha drainage basin is situated in northwest Guizhou, which is a typical karst peak-cluster depression region. The area exhibits unique hydrogeological structures, thin and discontinuous surface soils, rapid hydrological processes, and uneven spatial distributions of water and land resources (Wang *et al*., 2004). Fragile eco-geological environments, together with anthropogenic interference, have led to severe rocky desertification in the region. Recently, the first stage of a comprehensive rocky desertification mitigation project has been completed, and has proven to be effective. However, related research is lagging behind project progress.

The drainage basin is higher in the west and lower in the east, and elevation ranges between 911 and 2330 m. Land use types include forest, orchard, farmland, grassland, commercial land, and industrial and mining storage. Most of the basin is covered by forests, which occupy 45% of the entire region, and orchards rank second (25%). Farmland and grassland cover relatively small areas. Because both commercial land and land for industry and mining are dominated by human activities, they are combined into one group. According to land use remote sensing data from 1990 to 2010, there have been no significant dynamic changes in land use in the Sancha River Basin. Changes in farmland, grassland, woodland, and unused land are between –0.2% and 9%.

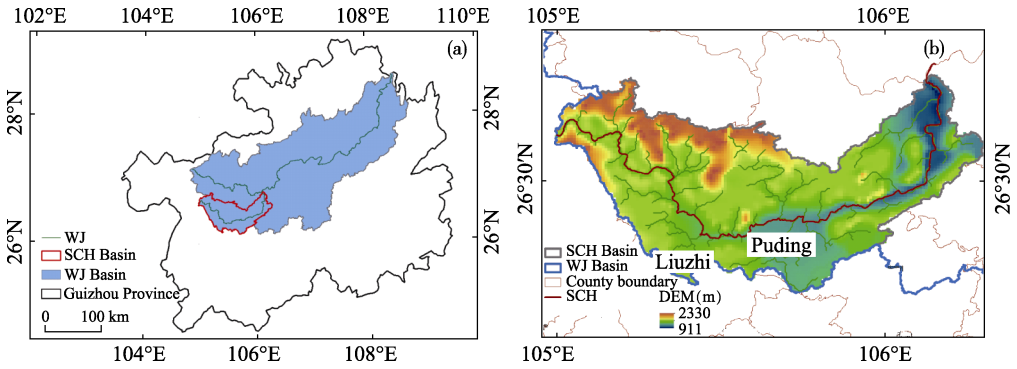

Figure 1 Map showing basic information of the Sancha River Basin (SCH: Sancha River; WJ: Wujiang River)

3 Materials and methods

3.1 Data preparation

Meteorological data, soil data, and DEM are the input data for the model simulation. Hydrologic data are used to verify the simulated effect. The rationality and accuracy of the input data are all very important for the simulation performance of the model.

3.1.1 Meteorological data

The meteorological database comprises daily measurements collected at Anshun weather station by the China Meteorological Data Service Center (http://cdc.cma.gov.cn/home.do). The database includes daily average temperature, precipitation, average wind speed, relative humidity, and sunshine duration. In addition, because this study focuses on runoff simulations, which are more prone to the influence of precipitation, four precipitation stations in the Sancha River Basin were selected for precipitation data. These stations are located at Bide, Machang, Santang, and Qibo. Measurements at the precipitation stations were collected from the Institute of Geographic Sciences and Natural Resources Research, Chinese Academy of Sciences (CAS): *Hydrological Yearbook of the People's Republic of China* – the Wujiang River Region of Yangtze River Basin. Basic information from weather and precipitation stations is shown in Table 1.

Table 1 Information for meteorological and rainfall stations

Station types	Station name	Latitude	Longitude	Elevation (m)	River system	Period
Meteorological station	Anshun	26°15′	105°54′	1431	—	Preheat year: 2006–2007; Calibration year: 2008–2010; Validation year: 2011–2013
Precipitation station	Bide	26°34′	105°10′	1500	—	
	Machang	26°19′	105°33′	1320	—	
	Santang	26°35′	105°33′	1588	—	
	Qibo	26°34′	106°10′	990	—	
Hydrological station	Yangchang	26°39′	105°11′	—	Sancha River	
	Longchangqiao	26°23′	105°47′	—	Sancha River	
	Hongjiadu	26°52′	105°52′	—	Liuchonghe	
	Yachihe	26°51′	106°09′	—	Wujiang River	

3.1.2 Hydrological data

According to the Yangtze River Basin record in the Hydrological Yearbook of the People's Republic of China (Ministry of Water Resources of the People's Republic of China), there are two hydrological stations in the Sancha River Basin: the Yangchang station and the Longchangqiao station, which are located in the upstream and midstream regions, respectively. Runoff data from hydrological stations in the discharge areas of the basin are required for model calibration, so Hongjiadu station (at the Liuchong River mouth) and Yachi station (in the mainstream of the Wujiang River, where the Liuchong River and Sancha River converge) were selected. Daily and monthly average runoff data from the Yangchang, Longchangqiao, Hongjiadu, and Yachi stations were used to calibrate and validate the SWAT model. Information about these stations is listed in Table 1.

3.1.3 Remote sensing data

Remote sensing data include digital elevation model (DEM) data, land use data, and soil data, which include soil types and associated physical and chemical properties. The Normalized Difference Vegetation Index (NDVI) was adopted for the spatial statistical analysis of runoff model simulation results. DEM data at 1 km resolution were obtained from the HYDRO1K database at the U.S. Geological Survey (USGS) EROS Center (http://eros.usgs.ov/#/Find_Data/Products_and_Data_Available/HYDRO1K). The 1:100,000 scale land use vector data of 2010 obtained from the Resources and Environmental Science Data Center, CAS (Liu *et al*., 2014) were applied. Soil data were collected from the Harmonized World Database version 1.1 (HWSD), established jointly by the Food and Agriculture Organization of the United Nations (FAO) and the International Institute for Applied System Analysis (IIASA) (Fischer *et al*., 2008). The main soil properties include soil type according to the FAO90 soil classification scheme, reference depth, and physical (such as gravel volume percentage, sand/silt/clay content, and effective moisture content) and chemical properties (namely organic carbon content and cation exchange capacity). NDVI data and the Moderate Resolution Imaging Spectroradiometer (MODIS) product (http://ladsweb.ascom. asa.gov/) from 2005–2010 were used, with temporal and spatial resolutions of 16 d and 500 m, respectively. Vegetation index data were mainly used to study the statistical spatial relationship between land cover and runoff generation in the river basin. NDVI in the Sancha River Basin is higher in the west and lower in the east, showing a banded spatial distribution (Figure 2).

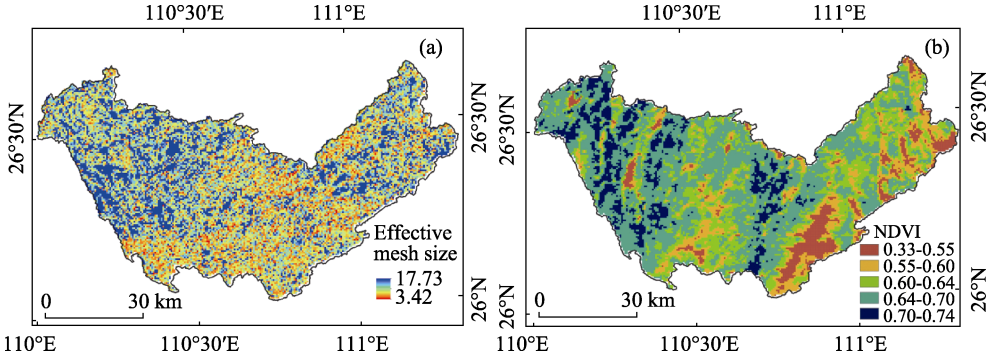

Figure 2 Spatial pattern of NDVI and index of landscape fragmentation in the Sancha River Basin

3.2 SWAT model introduction

This study used the SWAT model, which was calibrated and validated using measured runoff data from hydrological stations. It was then utilized to simulate runoff generation in a typical karst river basin, including total runoff, surface runoff, and groundwater runoff. The water cycle in the model was based on various hydrological variables:

$$SW_t = SW_0 + \sum_{i=1}^{t}(R_{day} - Q_{surf} - E_a - W_{seep} - Q_{gw}) \quad (1)$$

where SW_t denotes the final soil moisture content (mm); SW_0 denotes the initial soil moisture content on the i th day (mm); t represents the time (d); R_{day} represents the precipitation on the ith day (mm); Q_{surf} is the surface runoff on the ith day (mm); E_a is the evapotranspiration

on the i the day (mm); W_{seep} denotes the water seepage from the soil profile to the vadose zone (mm); and Q_{gw} denotes the baseflow returned on the i th day (mm).

Compared to other hydrological models (distributed and conceptual hydrologic models), the SWAT model is more favorable because it is based on hydrological processes and is more efficient due to easily obtained parameters. For example, the MIKE SHE hydrological model comprehensively considers hydrological processes, boundary conditions, and the spatial heterogeneity of collective characteristics in river basins; however, it is difficult to collect data on underlying surfaces and hydrogeological conditions (McMichael *et al*., 2006). The TOPMODEL model has a simple structure and demands fewer parameters, but it does not thoroughly consider the spatial heterogeneity of hydrological elements, and the coupled relationships between hydrological units (Beven *et al*., 1984). In the SWAT model, runoff simulation is performed using different modules (surface runoff, groundwater, and river confluence). For surface runoff, this study employs the relatively mature SCS curve number method (empirical model), which is a function of soil permeability, land use, and antecedent soil moisture conditions. The soil permeability is predominantly calculated according to the physical and chemical properties of different soil types in the karst area, which can reasonably reflect actual soil permeability in the region. Different land use types will affect runoff by changing surface evaporation, soil moisture conditions, and interception of land cover. As an input data point, the land use types in the river basin are eventually reflected by the SCS curve number. Studies have indicated that surface runoff will occur after the precipitation depth reaches 40 mm in karst areas (Peng and Wang, 2012). Therefore, antecedent soil moisture conditions are also a key factor influencing surface runoff in typical karst river basins. Groundwater runoff was calculated using water mass balance equations of shallow and deep aquifers. The volume was calculated based on different movement processes, and each module was controlled by the corresponding parameters. Groundwater runoff simulation results in karst areas are generally affected by factors such as the baseflow alpha factor (ALPHA_BF, a direct indicator of groundwater runoff in response to recharge variations) and threshold water depth in the shallow aquifer for flow (GWQMN).

3.2.1 Data preparation and model construction

(1) Construction of spatial database

Coordinate systems of different spatial data were consolidated (Krasovsky_1940_Albers) through ArcGIS using the .img data format. According to the land use data classification in the SWAT model, land use raster data were re-classified and converted to codes defined by the model. The 1:1,000,000 soil data for the Sancha River Basin underwent projection conversion, and special situations in the attribute tables were determined according to previous research experience.

(2) Preparation of attribute database

Soil database. The major parameters required by “USERSOIL” in the SWAT database are soil physical and chemical properties. Physical properties include mechanical composition, saturated hydraulic conductivity, and available water capacity, and chemical properties include organic carbon content, electrical conductivity, and others. Some parameters were obtained from the HWSD soil database, for example, soil layer thickness and organic carbon content, and saturated hydraulic conductivity and available water content were calculated using software (SPAW) or empirical equations.

Meteorological database. For each weather station, the .DBF documents of daily precipitation, daily maximum and minimum temperatures, solar radiation, average wind speed, and relative humidity were established. Meanwhile, a geographic information document (.DBF) of weather and precipitation stations was created to link the location map of the weather stations with the meteorological database.

Land use and soil index table. The index table links the SWAT attribute data with the spatial distribution maps of land use and soil type.

3.2.2 Sensitivity analysis and parameter calibration of SWAT model

This study utilizes measured runoff data from the Yangchang, Longchangqiao, Yachi, and Hongjiadu hydrological stations for parameter sensitivity analyses and model calibration and validation. Parameter sensitivity analyses were performed using the LH-OAT method embedded in the model and measured runoff data from hydrological stations. The results are shown in Table 2, which demonstrates that the most influential parameters for the runoff simulation were: the initial curve number (II) value (CN_2), which controls surface hydrological processes under soil moisture condition II (moderately moist soils); available water capacity (SOL_AWC); the soil evaporation compensation factor (ESCO); maximum canopy storage (CANMX); baseflow alpha factor (ALPHA_BF), which controls subsurface hydrological processes; the groundwater delay time (GW_DELAY); threshold water depth in the shallow aquifer for flow(GWQMN); and channel effective hydraulic conductivity (CH_K_2), which controls the main stream confluence. Based on the parameter sensitivity results and actual hydrological processes, the adjustable parameters were CN_2, SOL_AWC, ALPHA_BF, GWQMN, and CH_K_2. These parameters were adjusted several times until the simulated values were close to the measured values. The final values for all parameters are listed in Table 2. For groundwater runoff, previous studies on subsurface hydrological processes in karst areas (recharge, runoff, and discharge) (Amatya *et al*., 2011; Chen *et al*., 2014) were examined. Parameters were adjusted and validated several times to ensure accurate simulation results. Eventually, ALPHA_BF and GWQMN were set to 0.048–0.5 and 1000, respectively.

Table 2 Results of the sensitivity analysis and parameter calibration for the SWAT model

Parameters			Sensitivity rank			Parameter value	
Physical significance	Code	Process	YC	LCQ	CK	Default range	Adjustment range
SCS runoff curve number under normal moisture conditions	CN_2 (.mgt)	Surface runoff	2	3	5	35–98	50–98
Soil available water content	SOL_AWC (.sol)	Soil moisture	9	11	8	0–1	0.05–0.16
Baseflow alpha factor	ALPHA_BF (.gw)	Groundwater	5	14	15	0–1	0.048–0.5
Threshold water level in the shallow aquifer for groundwater to enter the main stream (mm)	GWQMN (.gw)	Groundwater	7	4	4	0–5000	1000
Channel effective hydraulic conductivity (mmh^{-1})	CH_K_2 (.rte)	Interflow	6	1	1	0–150	0–25

The Nash-Sutcliffe efficiency, E_{ns}, coefficient of determination, r^2, and hydrograph based on measured monthly runoff data for 2008–2010 were applied to evaluate the efficiency of the model and validate the calibration results. E_{ns} values closer to 1 indicate simulation val-

ues that are closer to the measured values. E_{ns} was calculated as follows:

$$E_{ns} = 1 - \frac{\sum_{i=1}^{n}(O_i - P_i)^2}{\sum_{i=1}^{n}(O_i - \overline{O})^2} \quad (2)$$

where O_i, O, P_i, and P are measured values, average measured values, simulated values, and average simulated values, respectively. It is generally believed that E_{ns} within 0.5–0.65 indicates acceptable simulation results. E_{ns} values of 0.65–0.75 and above 0.75 signify relatively good and excellent simulation results, respectively (Popov, 1979).

The results suggest that simulated monthly average precipitation at Longchangqiao station matches the measured values relatively well during the calibration period, with an E_{ns} of 0.82 and an R^2 of 0.92 (Figure 3 and Table 3). During the validation period, E_{ns} and R^2 are 0.90 and 0.93, respectively. The simulation agrees well with the measurement at Yangchang station during both calibration and validation periods, with corresponding E_{ns} values of 0.70 and 0.73. The simulation results are thus relatively good. In addition, from the hydrograph, the simulated and measured values at Yangchang and Longchangqiao stations are relatively coherent. Furthermore, simulation results at the basin outlet of both stations are not as good as those of Longchangqiao and Yangchang stations. The measured runoff in the discharge areas is estimated based on the difference between Yachi and Hongjiadu stations, which may contribute to the partial discrepancy.

Table 3 Statistical indicators of model performance at the three different monitoring stations of the Sancha River Basin

Hydrological stations	Calibration period (2008–2010)		Validation period (2011–2013)	
	E_{ns}	R^2	E_{ns}	R^2
Yangchang	0.70	0.84	0.73	0.93
Longchangqiao	0.82	0.92	0.90	0.95
Basin outlet	0.64	0.92	0.50	0.78

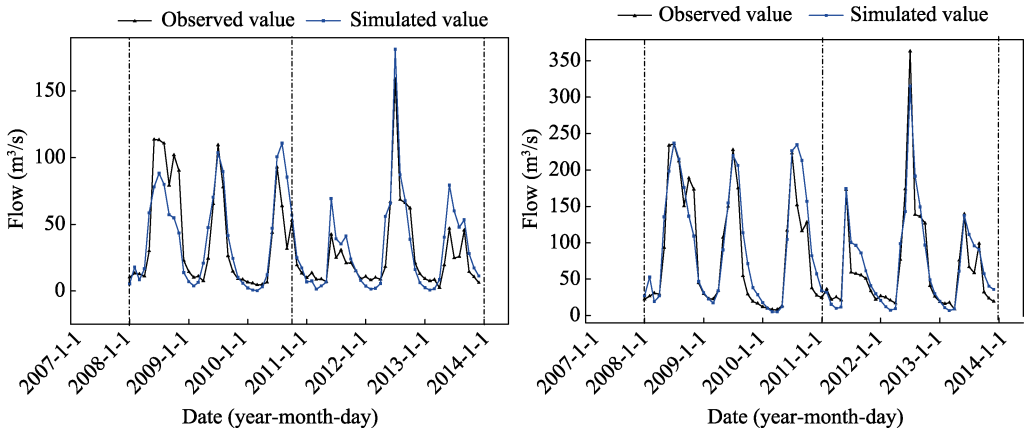

Figure 3 Simulated and observed monthly runoff at Yangchang (left) and Longchangqiao (right) station (Calibration period: 2008–2011; Verification period: 2011–2014)

3.3 Landscape fragmentation index

This study used the NDVI vegetation index to examine the spatial heterogeneity of runoff

generation, and the land use landscape fragmentation index to explain the spatial relationship between runoff service spatial heterogeneity and runoff volumes. The degree of landscape fragmentation was measured using the effective mesh size (Jaeger, 2000), which refers to the average value of the continuous area of each land use type in a landscape. A small value denotes a less fragmented landscape. The landscape fragmentation index can spatially reflect the intensity of land use type variations among different hydrological response units (HRUs). In more fragmented areas, there are remarkable differences in land use types between neighboring HRUs. The index integrates ecological processes, landscape compositions, and spatial patterns, and can therefore comprehensively and objectively express the degree of fragmentation (Gao and Cai, 2010). The equation is as follows:

$$m_{eff}(j) = A_j \cdot \sum_{i=1}^{n} (\frac{A_{ij}}{A_j})^2 = \frac{1}{A_j} \sum_{i=1}^{n} A_{ij}^{\ 2} \tag{3}$$

where $m(j)$, n, A_{ij}, and A_j denote the effective mesh size of landscape j, the number of complete patches in landscape j, the area of patch i in landscape j, and the area of landscape j, respectively. If the minimum of the index equals the size of the grid, it indicates that land use types are different for all neighboring grids. If the maximum equals the landscape area, it suggests that the landscape is of a homogeneous type. This study used the 'moving window' analysis (research amplitude) in the landscape pattern analyzing software FRAGSTATS (McGarigal and Marks, 1995) to compute the effective mesh size.

Based on the 30-m land use data (2010) in the Sancha River Basin (Figure 2b), it demonstrates that areas with high and low landscape fragmentation indices are scattered all over the region. The total area of low-value (highly fragmented) regions is larger than that of high-value regions. High-value areas are mainly located along the upstream region with higher elevations and less anthropogenic interference. Low-value areas are concentrated in the mid- and downstream regions.

3.4 Geographically weighted regression

Geographically Weighted Regression (GWR), proposed by Brunsdon *et al*. (1996; 1998), is a simple and practical local spatial analysis technique. GWR depicts the internal spatial relationships in the study area. In this study, it was used to reveal the spatial relationships of runoff volume with landscape fragmentation indices and the NDVI vegetation index under linear non-stationary conditions. The GWR model is an extension of the traditional regression model. It uses the spatial locations of data as one of the parameters, and evaluates spatial variations in independent variable–dependent variable relationships through using parameters.

The basic form of the GWR model is:

$$y_i = \beta_0(\mu_i, \nu_i) + \sum_{k=1}^{p} \beta_k(\mu_i, \nu_i) x_{ik} + \varepsilon_i \tag{4}$$

where (μ_i, ν_i) and k represent the coordinates of the ith sampling point and the number of independent variables, respectively; y_i, x_{ik}, and ε_i are the independent variables (total, surface, and groundwater runoff volumes), dependent variables (landscape fragmentation index and NDVI), and random errors at regression point i, respectively. $\beta_0(\mu_i, \nu_i)$ and $\beta_k(\mu_i, \nu_i)$ denote the intercept and slope of the GWR model at regression point i, respectively. The parameters can

be estimated using the following formula:

$$\beta(\mu_i, \nu_i) = (X^T W(\mu_i, \nu_i) X)^{-1} X^T W(\mu_i, \nu_i) Y \tag{5}$$

where $\beta(\mu_i, \nu_i)$ and $W(\mu_i, \nu_i)$ are, respectively, the unbiased estimator of the regression coefficient and the spatial weighting matrix, which is the core of the GWR model; the weight increases when the observation point is closer to the defined point. X and Y are the matrices for independent and dependent variables, respectively.

The Gaussian Spatial Weight function is universal, and its expression formula is as follows:

$$\omega_{ij} = \exp\left(-\frac{d_{ij}^2}{b^2}\right) \tag{6}$$

where ω_{ij}, $d_{ij,}$ and b denote the weight of observation point j, the Euclidean distance between regression point i and observation point j, and the non-negative attenuation parameter describing the weight-distance function relationship (also called bandwidth), respectively. When the distance between observation points is greater than b, the weight rapidly approaches 0.

4 Results and analysis

4.1 Spatial pattern of runoff services in the Sancha River Basin

The spatial patterns of runoff generation in the Sancha River Basin, including total runoff volume (TOTAQ), surface runoff (SURQ), and groundwater runoff (GWQ), are obtained using the SWAT model. In addition, because evapotranspiration significantly affects water balance, this study also analyzes the simulation results of actual evapotranspiration (ET). The average total runoff volume over the study period is higher in the north and lower in the south of the Sancha River Basin (Figure 4a), and fluctuates within 510–1177 mm, with an average of 826.4 mm. The total runoff coefficient reaches 70%. Areas with higher total runoff volumes (900–1100 mm) are mostly located in the east and the north, and cover 22% of the basin. The total runoff volume in the south of the basin is smaller and mostly within 500–700 mm.

The overall surface runoff is relatively low in the river basin, with an average value of 276 mm, and shows remarkable spatial heterogeneity. The surface runoff coefficient is 23.9%. Surface runoff in 50% of the river basin is between 0 and 300 mm, and mainly located in the southern portion. Areas with more than 300 mm runoff are scattered in the east and the north. This is because the Sancha River Basin is situated in a typical karst area, and surface runoff patterns are highly heterogeneous. The unique surface-subsurface binary hydrological structures cause a considerable amount of surface water loss to the subsurface. Hence, there is relatively abundant subsurface runoff in the river basin (Figure 4c). Approximately 60%–70% of the region has an underground runoff volume of 500–700 mm. Underground runoff volume in upstream areas is typically over 500 mm.

The actual evapotranspiration amounts show no significant differences over the river basin. Most areas in upstream and downstream regions experience evapotranspiration of 100–300 mm (Figure 4d), covering 53% of the total area. Evapotranspiration is 300–500 mm in certain parts of central and southern regions. Compared to the spatial patterns of different runoff types, the distribution of actual evapotranspiration is relatively homogeneous in the Sancha River Basin. This is because evapotranspiration is mostly influenced by temperature,

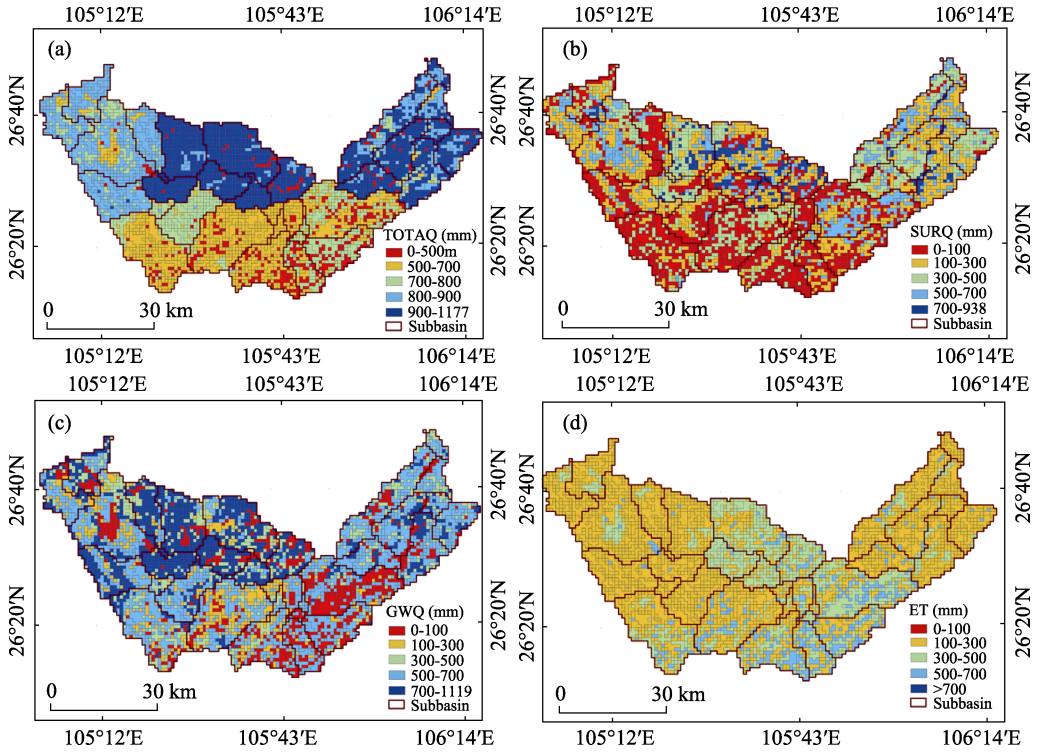

Figure 4 Spatial pattern of TOTAQ (a), SURQ (b), GWQ (c), and ET (d) in the Sancha River Basin

precipitation, wind speed, and vegetation type (Borba *et al*., 2012). The DEM data (Figure 1) show 70% of the area is within the range of 900 to 1500 m and no remarkable differences in temperature and wind speeds over the study area. Coniferous forests and shrubs are the dominant vegetation types (more than 80%), which results in relatively low spatial heterogeneity of evapotranspiration.

4.2 Gradient analysis of runoff generation based on topographic factors

Elevation in the Sancha River Basin ranges between 911 and 2330 m. The corresponding average values and coefficients of variation for the total runoff volume, surface runoff, underground runoff, and actual evapotranspiration at elevation gradients of 911–1000 m, 1000–1500 m, and 1500–2330 m are obtained. Figure 4 and Table 4 show that variations in the total runoff volume with elevation are small (803–882 mm), and fluctuations in the coefficient of variation are insignificant (0.09–0.21), while surface runoff variations are relatively large. At elevations of 911–1000 m, the surface runoff is 401 mm and the coefficient of variation is 0.52. As the elevation increases, the surface runoff decreases to 154 mm and the coefficient of variation increases to 0.85. The average value of underground runoff gradually increases at higher elevation. The actual evapotranspiration exhibits no difference at different elevation gradients. In general, elevation has significant effects on surface and underground runoff in the Sancha River Basin. The percentage of underground runoff increases with elevation, while that of surface runoff decreases.

The gradient analysis of slope (Table 4) indicates that the total runoff volume increases on steeper slopes. The surface runoff first increases and then decreases with increasing slope. It

reaches a maximum (319 mm) on slopes from 5–10°. For a slope range of 0–10°, the surface runoff increases with slope. The force in the water layer along the slope surface increases, and the pressure perpendicular to the slope surface decreases. This leads to a smaller infiltration rate and greater surface runoff. As the slope becomes steeper, the vertical action force exerted by precipitation on the ground surface is smaller, and soil crust formation is slower, resulting in less surface runoff. This is similar to the law of runoff generation on karst slopes studied by Hu *et al*. (2012), whereby groundwater runoff essentially increases on steeper slopes. The highest runoff value is 629 mm. For steeper slopes, the vertical action force exerted by precipitation on the ground surface is smaller, and underground runoff increases at slower rates (Wu and Zhang, 2006). In different slope ranges, the average actual evapotranspiration fluctuates between 222 and 259 mm.

Table 4 Runoff and evapotranspiration based on different elevations of hydrological response units (HRUs) in the Sancha River Basin

Terrain factors			Total flow (mm)		Surface runoff (mm)		Groundwater (mm)		Evapotranspiration (mm)	
Element	Gradient	Percentage area	Average	CV	Average	CV	Average	CV	Average	CV
Elevation (m)	911–1000	1.8%	882	0.09	401	0.52	481	0.52	212	0.28
	1000–1500	64.2%	803	0.17	310	0.75	493	0.48	251	0.27
	1500–2330	34.0%	882	0.15	154	0.85	591	0.42	245	0.27
Slope (°)	0–5	61.9%	825	0.17	301	0.80	523	0.46	253	0.27
	5–10	24.5%	838	0.16	319	0.72	519	0.46	241	0.27
	10–15	12.3%	881	0.15	303	0.75	578	0.49	227	0.27
	15–24	1.3%	863	0.21	233	0.85	629	0.44	222	0.28

4.3 Spatial statistical relationship between land cover and runoff services

4.3.1 Statistical characteristics of runoff services under different land cover conditions

Vegetation cover influences runoff by reducing the kinetic energy of raindrops, intercepting precipitation, modifying soil crusts, and altering soil infiltration capacity (Wu and Zhang, 2006). The total runoff volumes are similar for the five land use types, and all fluctuations are within 718–850 mm. Total runoff volumes for grassland are slightly lower. There are relatively significant differences in surface and underground runoff among the different land use types. In particular, industrial and commercial land experiences the highest surface runoff (544 mm), followed by farmland. Commercial and industrial land is dominated by heavy human activities and impermeable layers in urban areas, which substantially weaken the capacity of soil to retain and store water. Consequently, most precipitation becomes surface runoff. Meanwhile, underground runoff shows the opposite trend. It accounts for more than 70% of the total runoff in orchard and forest land underground, and is the highest in forests (628 mm). Soils in forests have better physical structures, higher permeability, and the litterfall excels at retaining water (Shi and Li, 2001). Moreover, forests are often located in higher-altitude and steeper regions.

Vegetation cover conditions affect the hydrological processes and runoff generation in the river basin by changing surface evaporation, soil moisture conditions, and interception of land cover. The NDVI in the Sancha River Basin is divided into three classes: <0.5, 0.5–0.7,

and >0.7, and the corresponding runoff for each NDVI gradient is analyzed. Figure 5 shows that the total runoff and underground runoff increase with higher NDVI, while the surface runoff increases at first but subsequently decreases (259-319-282 mm). This is because improved vegetation cover conditions reduce with limits resulting in water loss, which is due to surface-subsurface binary hydrological structures. As NDVI continues to rise, interception by the vegetation canopy increases and transpiration becomes stronger, and the soils can retain and store more water, which decreases surface runoff.

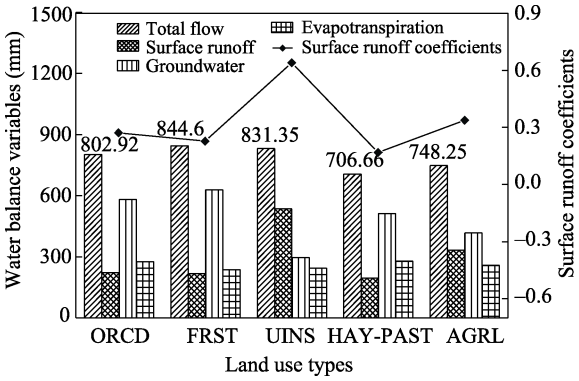

NDVI	<0.5	0.5–0.7	>0.7
Total flow (mm)	794	830	835
Surface runoff (mm)	259	319	282
Groundwater (mm)	535	523	565
Evapotranspiration (mm)	230	296	277

Figure 5 Runoff generation of different land use types in the Sancha River Basin

4.3.2 Spatial correlation between landscape fragmentation, vegetation cover, and runoff generation

Based on the GWR model, the landscape fragmentation index (m_{eff}), and NDVI, the local spatial relationships between land cover and different runoff volume variations are analyzed at the HRU scale (Figure 6). To ensure accurate characterization of macroscopic patterns and local details over the entire study area, R^2 and residual sum of squares of regression models are employed as criteria to determine the optimal bandwidth, which is 7 km. The Gaussian function is selected as the weight function. The total runoff volume and the landscape fragmentation index in the Sancha River Basin show mostly positive correlations. Areas with positive correlations occupy 96.5% of the entire region. Negative correlations mainly occur in limited areas in the southeast. Areas with strong positive spatial correlations are located in the south and northeast. The spatial regression relationship between underground runoff volume and the landscape fragmentation index is similar to that of the total runoff volume. 99.9% of the river basin shows positive correlations, and correlations gradually weaken from west to east. A relatively heterogeneous spatial relationship is noted between surface runoff and the landscape fragmentation index; they are mostly negatively correlated (74.2%) in western and central regions. Positive correlations are only observed in limited areas in the east and north. The actual evapotranspiration volume and the landscape fragmentation index demonstrate negative spatial correlations overall (96.9%).

The spatial non-stationary relationship of the GWR regression coefficient between NDVI and runoff shows remarkable differences in the south and west (Figure 7). In the upstream and midstream regions of the Sancha River Basin, the total runoff volume and NDVI are mostly positively correlated, which accounts for 61.4% of the entire basin. The correlations become negative in the north and the downstream region. The spatial relationship between surface runoff and NDVI is relatively complex, and the positively and negatively correlated

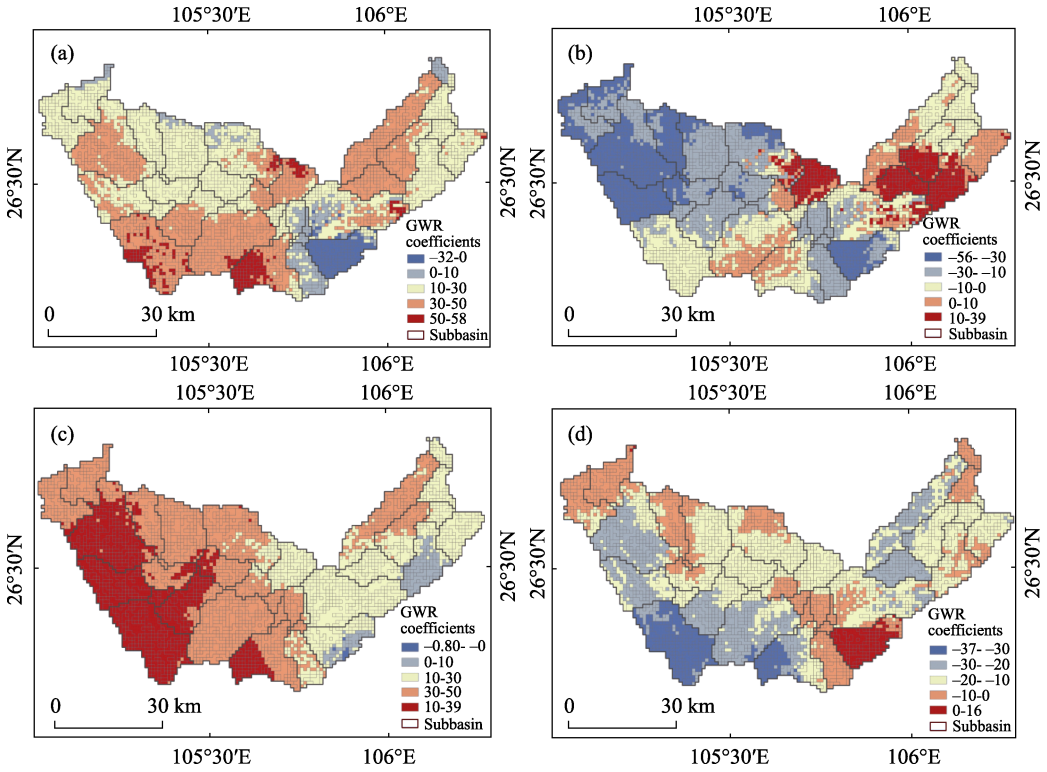

Figure 6 Spatial pattern of regression coefficients using the GWR model of the landscape fragmentation index and water balance components in the Sancha River Basin (a. total flow, b. SURQ, c. GWQ, d. ET)

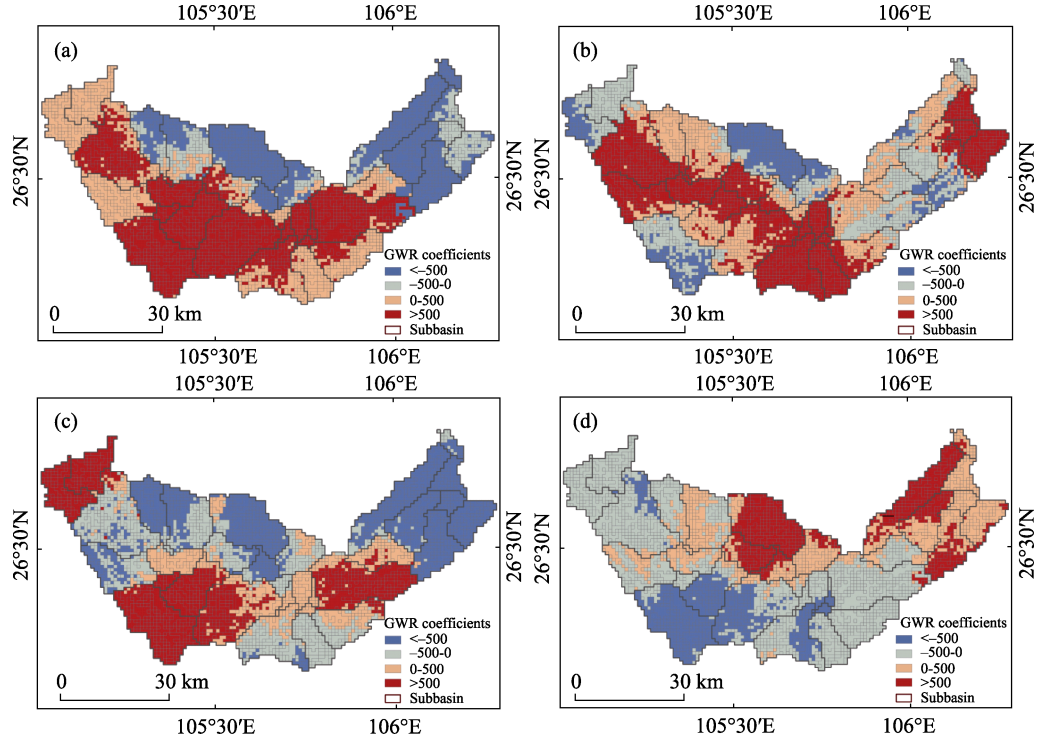

Figure 7 Spatial pattern of regression coefficients using the GWR model of the NDVIand water balance components in the Sancha River Basin (a. TOTAQ, b. SURQ, c. GWQ, d. ET)

areas are scattered throughout the basin. The positively correlated areas cover 67.3% of the entire region, and are mostly located in the western and central regions as well as the outlet of the basin. The underground runoff demonstrates negative correlations with NDVI for 56.4% of the basin. Figures 6 and 7 jointly suggest that areas with relatively better ecological background in the upstream region have higher elevation, less landscape fragmentation, greater NDVI, higher total runoff volume, more underground runoff, and less surface runoff. This indicates relatively effective ecological restoration. 52.5% of the basin shows negative correlations between actual evapotranspiration and NDVI, predominantly in the south and upstream regions.

5 Conclusions and discussion

Based on the calibrated SWAT model, the runoff services of typical karst basin were simulated, and the spatial variability of different services were analyzed along with the methods of gradient analysis and local regression. The applicability of the SWAT model to the Sancha River Basin was enhanced through sensitivity analyses and parameter calibration. The simulated average total runoff volume is higher in the north and lower in the south, and the total runoff coefficient of the basin is 70%. The surface runoff demonstrates remarkable spatial heterogeneity, and the overall value is relatively low. There is abundant underground runoff, which is closely related to the typical karst topography and surface-subsurface binary hydrological structures. Higher elevations and steeper slopes increase the percentages of total runoff and underground runoff. Vegetation cover conditions impose different influences on runoff generation. Relatively significant differences exist among the effects of vegetation cover types on surface runoff and underground runoff. NDVI is mostly positively correlated with surface runoff generation. Together with the influence of vegetation cover, steeper slopes cause surface runoff to first increase and then decrease. Spatial overlay analyses indicate that total runoff and underground runoff attain their maximum values in forests. This is because forest ecosystems have a stronger soil moisture retention capacity, and water can rapidly infiltrate into the soils in the study area. Moreover, because forests are mainly located at higher elevation, and the slopes are relatively steep, underground runoff is formed easily.

To summarize, in upstream regions of the Sancha River Basin, elevation is the dominant factor affecting total runoff volume and underground runoff, while land cover conditions determine the surface runoff volume. In downstream regions, both topography and elevation affect the total runoff volume and underground runoff. Specifically, orchards (56% of the total area) play an important role in retaining water and modifying evapotranspiration, affecting surface runoff. By studying runoff generation in a typical karst river basin, and their spatial variation characteristics, it is concluded that specifically designed ecological restoration measures (Grain to Green Project in upstream regions, and garden construction in downstream regions) can enhance the total water retention in the region, and reduce the surface runoff volume, therefore strengthening the regional soil conservation capability. Eventually, the capacity of carbon fixation in forests in upstream regions will increase, and the wellbeing for downstream areas can be improved.

This study makes full use of the fact that a semi-distributed hydrological model (SWAT) is based on hydrological processes and requires easily obtainable input data. The most influential parameters for runoff simulation in karst river basins, namely CN_2 and

ALPHA_BF, were adjusted to attain a final Nash-Sutcliffe efficiency above 0.7. The objective of this study was to analyze the spatial patterns of runoff in the Sancha River Basin, and the spatial statistical relationships with different environmental factors. After parameter calibration and validation, the SWAT model can effectively achieve this goal. Therefore, the SWAT model was employed to simulate the spatial patterns of runoff generation services during the study period. Subsequently, based on the quantification of landscape fragmentation, the GWR model was used to quantitatively examine the spatial correlations between land cover conditions and runoff generation. This study therefore fills the gap in previous research that solely analyzed runoff characteristics based on statistical surveys on different land use types and landscape indices (Lin *et al*., 2014), and which lacked information on relevant macroscopic patterns. Moreover, although the SWAT model provides superior simulation results after parameter calibration and validation, it is hard to completely avoid equifinality due to the extremely complex hydrological processes and hundreds of parameters involved. It is possible that the final simulation results are satisfactory only because some combinations of parameters reach the ideal levels. Hence, in future, meticulous optimization of hydrological process simulation should be performed, considering the special hydrogeological conditions in karst areas, so that the model better depicts actual hydrological processes in the study area.

Acknowledgements

All the authors thank the Data Center for Resources and Environmental Sciences, Chinese Academy of Sciences (RESDC) and EOS/Terra of National Aeronautics and Space Administration, for producing and sharing the land use and NDVI dataset, respectively.

References

Amatya D M, Jha M, Edwards A E *et al*., 2011. SWAT-based streamflow and embayment modeling of karst-affected chapel branch watershed, South Carolina. *Transactions of the ASABE*, 54(4): 1311–1323.

Bai Xiaoyong, Wang Shijie, 2011. Relationships between soil loss tolerance and karst rocky desertification. *Journal of Natural Resources*, 26(8): 1315–1322. (in Chinese)

Beven K J, Kirkby M J, Schofield N *et al*., 1984. Testing a physically-based flood forecasting model (TOPMODEL) for three U.K. catchments. *Journal of Hydrology*, 69(1): 119–143.

Borba B S M C, Szklo A, Schaeffer R, 2012. Plug-in hybrid electric vehicles as a way to maximize the integration of variable renewable energy in power systems: The case of wind generation in northeastern Brazil. *Energy*, 37(1): 469–481.

Brunsdon C, Fotheringham A S, Charlton M, 1996. Geographically weighted regression: A method for exploring spatial nonstationarity. *Geographical Analysis*, 28(4): 281–298.

Brunsdon C, Fotheringham A S, Charlton M, 1998. Geographically weighted regression: Modelling spatial non-stationarity. *Journal of the Royal Statistical Society Series D*: *The Statistician*, 47(3): 431–443.

Chen Hongsong, Nie Yunpeng, Wang Kelin, 2013. Spatio-temporal heterogeneity of water and plant adaptation mechanisms in regions: A review. *Acta Ecologica Sinica*, 33(2): 317–326. (in Chinese)

Chen Xi, Zhang Zhicai, Rong Li *et al*., 2014. Process of Water Cycle and Effect of Eco-hydrology in the Karst Region of Southwestern China. Beijing: Science Press. (in Chinese)

Costanza R, D'Arge R, Groot R D *et al*., 1997. The value of the world's ecosystem services and natural capital. *Nature*, 387(15): 253–260.

Dai Quanhou, Peng Xudong, Yang Zhi *et al*., 2017. Runoff and erosion processes on bare slopes in the karst rocky desertification area. *Catena*, 152: 218–226.

Daily G C, 1997. Nature's Services: Societal Dependence on Natural Ecosystems. Washington, DC: Island Press.

Fischer G F, Nachtergaele S, Prieler H T *et al*., 2008. Global agro-ecological zones assessment for agriculture (GAEZ 2008). IIASA, Laxenburg, Austria and FAO, Rome, Italy.

Fu Bojie, Wang S, Su C H *et al*., 2013. Linking ecosystem processes and ecosystem services. *Current Opinion in*

Environmental Sustainability, 5(1): 4–10.
Fu Bojie, Yu Dandan, 2016. Trade-off analyses and synthetic integrated method of multiple ecosystem services. *Resources Science*, 38(1): 1–9. (in Chinese)
Fu Bojie, Zhang Liwei, 2014. Land-use change and ecosystem services: Concepts, methods and progress. *Progress in Geography*, 33(4): 441–446. (in Chinese)
Gao Jiangbo, Cai Yunlong, 2010. Spatial heterogeneity of landscape fragmentation at multi-scales: A case study in Wujiang river basin, Guizhou Province, China. *Scientia Geographica Sinica*, 30(5): 742–747. (in Chinese)
Hu Yi, Dai Quanhou, Wang Peijiang, 2012. Runoff features and the influencing factors on karst sloping farmland. *Journal of Soil and Water Conservation*, 26(6): 46–51. (in Chinese)
Jaeger J A G, 2000. Landscape division, splitting index, and effective mesh size: New measures of landscape fragmentation. *Landscape Ecology*, 15(2): 115–130.
Li Shuangcheng, 2014. The Geography of Ecosystem Services. Beijing: Science Press. (in Chinese)
Li Zhou, Gao Kaimin, Liu Jinchun *et al*., 2016. Growth response of two annual herb species to alternating drying-wetting and nitrogen addition in the karst area of Southwest China. *Acta Ecologica Sinica*, 36(11): 3372–3380. (in Chinese)
Lin Bingqing, Chen Xingwei, Chen Ying *et al.*, 2014. Simulations and analysis on the effects of landscape pattern change on flood and low flow based on SWAT model. *Acta Ecologica Sinica*, 34(7): 1772–1780. (in Chinese)
Liu Changming, Du Wei, 1985. An application of system analysis to water allocation in the first-stage project of the east-route water transfer in China. *Geographical Research*, 4(3): 81–88. (in Chinese)
Liu Jiyuan, Kuang Wenhui, Zhang Zengxiang *et al.*, 2014. Spatiotemporal characteristics, patterns and causes of land use changes in China since the late 1980s. *Acta Geographica Sinica*, 69(1): 3–14. (in Chinese)
Lv Leting, Peng Qiuzhi, Guo Yuanyuan *et al.*, 2014. Runoff simulation of Dongjiang river basin based on the soil and water assessment tool. *Journal of Natural Resources*, 29(10): 1746–1757. (in Chinese)
Mcgarigal K, Marks B J, 1995. FRAGSTATS: Spatial analysis program for quantifying landscape structure. Dolores Po Box, 351.
Mcmichael C E, Hope A S, Loaiciga H A, 2006. Distributed hydrological modeling in California semi-arid shrublands: MIKESHE model calibration and uncertainty estimation. *Journal of Hydrology*, 317(3): 307–324.
Millennium Ecosystem Assessment (MEA), 2005. Ecosystems and Human Well-Being. Washington DC: Island Press.
Pan Shibing, Lu Jingxuan, 2010. Karst groundwater exploitation in Southwest and countermeasure to cope with drought. *China Water Resources*, 13: 40–42. (in Chinese)
Peng T, Wang S J, 2012. Effects of land use, land cover and rainfall regimes on the surface runoff and soil loss on karst slopes in southwest China. *Catena*, 90(1): 53–62.
Popov E G, 1979. Gidrologicheskie Progonozy (Hydrological Forecasts). Leningrad: Gidrometeoizdat.
Shi Peili, Li Wenhua, 2001. Influence of forest cover change on hydrological process and watershed runoff. *Journal of Natural Resources*, 16(5): 481–487. (in Chinese)
Southwestern China. Beijing: Science Press, 2014. (in Chinese)
Tian Y, Wang S, Bai X *et al.*, 2016. Trade-offs among ecosystem services in a typical karst watershed, SW China. *Science of the Total Environment*, s566/567: 1297–1308.
Wang S J, Liu Q M, Zhang D F, 2004. Karst rocky desertification in southwestern China: Geomorphology, land use, impact and rehabilitation. *Land Degradation & Development*, 15(2): 115–121.
Wang X Z, Liang Z X, Wang J, 2014. Simulation of runoff in karst-influenced Lianjiang Watershed using the SWAT model. *Scientific Journal of Earth Science*, 4(2): 85–92.
Wu Xiyuan, Zhang Liping, 2006. Research on effecting factors of precipitation's redistribution of rainfall intensity, gradient and cover ratio. *Journal of Soil and Water Conservation*, 20(4): 28–30. (in Chinese)
Xu H, Xu C Y, Sælthun N R *et al.*, 2015. Entropy theory based multi-criteria resampling of rain gauge networks for hydrological modelling: A case study of humid area in southern China. *Journal of Hydrology*, 525(A): 138–151.
Yuan Daoxian, 2015. Scientific innovation in karst resources and environment research field of China. *Carsologica Sinica*, 34(2): 98–100. (in Chinese)
Zhang Mingyang, Wang Kelin, Liu Huiyu *et al.*, 2011. The response of ecosystem service values to ambient environment and its spatial scales in typical karst areas of northwest Guangxi, China. *Acta Ecologica Sinica*, 31(14): 3947–3955. (in Chinese)
Zhang Z, Chen X, Huang Y *et al.*, 2013. Effect of catchment properties on runoff coefficient in a karst area of southwest China. *Hydrological Processes*, 28(11): 3691–3702.
Zhou F, Xu Y, Chen Y *et al.*, 2013. Hydrological response to urbanization at different spatio-temporal scales simulated by coupling of CLUE-S and the SWAT model in the Yangtze River Delta region. *Journal of Hydrology*, 485: 113–125.